

NONLINEAR REGRESSION PROBLEM OF MATERIAL FUNCTIONS IDENTIFICATION FOR POROUS MEDIA PLASTIC FLOW

Z. N O W A K¹ and A. S T A C H U R S K I²

¹ **Institute of Fundamental Technological Research,**
Świętokrzyska 21, 00-049 Warsaw, Poland

² **Institute of Control and Computation Engineering,**
Warsaw University of Technology, Warsaw, Poland

In the paper we present the identification problem arising in modelling the processes of nucleation and growth of voids in the elastic-plastic media. Identification is carried out on the basis of Fisher's data measured on the cylindrical steel specimens subjected to the uniaxial tension. The identification problem is formulated as the standard nonlinear regression problem. Our aim was to select appropriate formulae of the material functions appearing in the porosity model in the right-hand side of the differential equation, and to identify their unknown parameters. The resulting nonlinear regression problem was solved by means of the global optimization method of Boender *et al.* As the local minimizer we have implemented the modified famous BFGS quasi-Newton method. Modifications were necessary to take into account box constraints posed on the parameters. As the directional minimizer we have prepared a special procedure joining quadratic and cubic approximations and including a new switching condition. We have tested two variants of the porosity model; in the first one with variable shape of the material function g , and the second one – with constant g . The results suggest that the model with material function $g \equiv 1$ describes well the nucleation and growth of voids. However, our attempt to identify that constant has brought an unexpected value smaller than 1, and approximately equal to 0.84.

Keywords: plastic flow of porous media, material functions identification, global optimization, nonlinear regression, nonlinear programming.*

1. INTRODUCTION

The model of the nucleation and growth phenomenon is assumed in the form of an ordinary differential equation connecting total porosity with the equivalent plastic strain. The right-hand side of the equation is the sum of two terms. The

*Paper was presented at 33rd Solid Mechanics Conference, 05-09.09.2000, Zakopane, Poland

first one represents the nucleation of voids and contains the material function h while the second represents the growth of voids and contains the material function g . Our aim was to select appropriate formulae of those material functions and identify their unknown parameters.

The identification problem is formulated as the standard nonlinear regression problem where we minimize the sum of squares of the differences between the calculated and measured porosity values, i.e. the mean squares function (see for details Sec. 2).

The resulting nonlinear regression problem was solved by means of the global optimization method of Boender *et al.* (see Subsec. 6.1). As the local minimizer we have implemented the modified, famous BFGS quasi-Newton method (see Subsec. 6.2). Modifications were necessary to take into account the box constraints posed on the parameters. As the directional minimizer we have elaborated a special procedure combining the quadratic and cubic approximations and including a new switching condition (see Subsec. 6.3).

We have tested two variants of the porosity model. The first one with variable shape of the material function g and the second one with constant g . In the second case we have assumed first $g \equiv 1$ and afterwards tried to identify the constant. To obtain the calculated porosity parameter, ξ , we had to solve the poorly conditioned differential evolution equation. Finally we have decided to solve it by means of the Rosenbrock method for stiff differential equations (see Subsec. 6.4).

The resulting least squares problem is introduced in Sec. 2. The material functions formulae are described in Subsec. 4. The data used for parameter estimation are presented in Sec. 5. The computational results are shown and discussed in Sec. 7. Some conclusions and observations are also stated.

In Tables 1a, 2a, 3a the "best" minima found for each interval are collected. The presentation of the whole set of local minima is restricted to three due to the lack of space (see Tables 1a, 2a and 3a). Finally, Sec. 8 contains some concluding remarks.

2. FORMULATION OF THE IDENTIFICATION PROBLEM

Our nonlinear regression problem is formulated as usual. We minimize the sum of squares of the differences between the calculated and measured porosity values, i.e. the mean squares function

$$(2.1) \quad \min_{x \in V} \|\mathbf{Y} - \tilde{\mathbf{Y}}\|^2,$$

where $V \subset \mathbb{R}^n$ denotes the set of admissible parameters values (n is the number of the unknown parameters to be identified). Substitution of the formula

$\tilde{Y}_i = F(\bar{\epsilon}_{pi}, x)$ into (2.1) yields

$$(2.2) \quad \min_{x \in V} \sum_{i=1}^M \{Y_i - F(\bar{\epsilon}_{pi}, x)\}^2.$$

Usually the LEVENBERG-MARQUARDT method (cf. LEVENBERG [11], MARQUARDT [12]) is used to minimize the mean squares function with respect to the unknown parameters to be estimated.

3. POROSITY MODEL

3.1. Porosity evolution at the neck

In the following considerations the uniaxial test is assumed for room temperature. We assume, following HILL [10], that after a neck has been formed in a cylindrical tensile specimen, the distribution of the stress across a transverse section is not uniform. Our analysis is based on the constitutive relation for the porous plastic solids. We put it into the form introduced by RUDNICKI and RICE [18].

We have assumed an augmented version of GURSON'S porous material model [9] with the following porosity evolution

$$(3.1) \quad \dot{\xi} = h \frac{1}{1 - \xi} \text{tr}(\sigma \mathbf{D}^p) + g(1 - \xi) \text{tr}(\mathbf{D}^p),$$

where h, g are the material functions, $\bar{\epsilon}_p$ is the equivalent plastic strain, σ is the Cauchy stress tensor, \mathbf{D}^p denotes the plastic rate of the deformation tensor.

We have simplified our set of differential equations assuming the Bridgman solution. As the result, to obtain the calculated porosity parameter we had to solve only one poorly conditioned differential evolution equation.

$$(3.2) \quad \frac{\dot{\xi}}{\dot{\epsilon}_p} = \left[h \frac{1}{1 - \xi} \left(\lambda_1 \frac{\sigma_{xx}}{\sigma_{zz}} + \lambda_2 \frac{\sigma_{yy}}{\sigma_{zz}} + 1 \right) + g(1 - \xi)(\lambda_1 + \lambda_2 + 1) \right] \frac{1}{\sqrt{\lambda^*}}$$

where

$$\lambda_1 = \frac{\dot{E}_{xx}^p}{\dot{E}_{zz}^p}, \quad \lambda_2 = \frac{\dot{E}_{yy}^p}{\dot{E}_{zz}^p} \quad \text{and} \quad \lambda^* = \frac{2}{3} [(\lambda_1)^2 + (\lambda_2)^2 + 1].$$

We assume that h and g are functions depending on plastic strain and unknown parameters.

3.2. Stress state at the neck

Further changes in the porosity model are introduced assuming the Bridgman solution for the stress state at the minimum section of the tensile specimen. Equation (3.2) is valid everywhere in the neck of the tensile cylindrical specimen. Therefore it suffices to identify material functions parameters in the central point of the neck. In what follows we shall restrict our considerations to that central point (with $x = y = z = 0$). According to Bridgman, the analytical expression for the stress depends on the matrix flow stress $\bar{\sigma}$ and the geometry of the neck – R/ρ_R , where R is the radius of the minimum section, and ρ_R is the neck contour radius

$$(3.3) \quad \left. \begin{aligned} \sigma_{xx} = \sigma_{yy} &= \bar{\sigma} \ln \left(\frac{R^2 + 2R\rho_R}{2R\rho_R} \right) \\ \sigma_{zz} &= \bar{\sigma} \left(1 + \ln \left(\frac{R^2 + 2R\rho_R}{2R\rho_R} \right) \right) \end{aligned} \right\} \quad \text{for } x, y, z = 0.$$

In general, the stress state in the minimum section in the neck, according to Bridgman, depends on the distance to the z axis. The distance to the z -axis does not appear in formulae (3.3) because we consider exclusively the central point of the neck.

We have assumed furthermore as in SAJE, PAN and NEEDLEMAN [19] that

$$(3.4) \quad \begin{aligned} \frac{R}{\rho_R} &= 0.833(\bar{\epsilon}_p - 0.2), & \text{for } \bar{\epsilon}_p \geq 0.2, \\ \frac{R}{\rho_R} &= 0.0, & \text{for } \bar{\epsilon}_p < 0.2. \end{aligned}$$

Taking Eq. (3.4) into account in the Bridgman solution, we obtain for axisymmetric tension

$$(3.5) \quad \frac{\sigma_{xx}}{\sigma_{zz}} = \frac{\sigma_{yy}}{\sigma_{zz}} = \lambda$$

where

$$(3.6) \quad \lambda = \ln \left(\frac{R^2 + 2R\rho_R}{2R\rho_R} \right) / \left(1 + \ln \left(\frac{R^2 + 2R\rho_R}{2R\rho_R} \right) \right).$$

Furthermore, we have assumed the constitutive relation for the porous plastic solids introduced by GURSON [9]. This constitutive relation can be put into the form introduced by RUDNICKI and RICE [18], $\dot{E}_{ij}^p = \frac{1}{H} P_{ij} Q_{kl} \bar{\sigma}^{kl}$, where $\bar{\sigma}$ is the Jaumann rate-of-change of the Cauchy stress. If we assume that the porous

material yields in accordance with the GURSON [9] criterion, the constitutive relation can be expressed as

$$(3.7) \quad \dot{E}_{ij}^p = \frac{1}{H} \left(\frac{3S_{ij}}{\bar{\sigma}^2} + \frac{\alpha}{\bar{\sigma}} \delta_{ij} \right) Q_{kl} \bar{\sigma}^{\nabla^{kl}},$$

where $S_{ij} = \sigma_{ij} - \frac{1}{3}\sigma_{kk}\delta_{ij}$ and

$$(3.8) \quad \alpha = \xi \sinh \left(\frac{\sigma_{kk}}{2\bar{\sigma}} \right).$$

Therefore finally for our coordinate system we obtain

$$(3.9) \quad \frac{\dot{E}_{xx}^p}{\dot{E}_{zz}^p} = \lambda_1 = \frac{\dot{E}_{yy}^p}{\dot{E}_{zz}^p} = \lambda_2 = \frac{3S_{xx} + \bar{\sigma}\alpha}{3S_{zz} + \bar{\sigma}\alpha}.$$

Precise calculation of H and Q_{kl} is not necessary because these quantities are eliminated from the above formulae.

4. MATERIAL FUNCTIONS

We have investigated many forms of the material functions h and g and their combinations. There exist certain requirements on the shape of the h function. As the first function satisfying them we have used the Gauss normal distribution function as proposed by CHU and NEEDLEMAN [4]. Usually in the literature, the material function g is taken to be equal to 1 also in models containing the nucleation part. We have allowed varying shape of the material function g as proposed in PERZYNA and NOWAK [15]. We have used the following formulae for the material function h :

- Gauss normal distribution function

$$(4.1) \quad h_1(\bar{\epsilon}_p, a_1, b_1, c_1) = \frac{a_1}{b_1\sqrt{2\pi}} \exp \left(-\frac{1}{2} \left[\frac{\bar{\epsilon}_p - c_1}{b_1} \right]^2 \right).$$

All parameters of function h have their mechanical meaning in that case. Namely, a_1 denotes the maximum value of the porosity parameter, b_1 is the width of the voids distribution region, and c_1 represents the value of the equivalent plastic strain $\bar{\epsilon}_p$ at the moment when the porosity parameter reaches its maximal value.

- Power exponent function

$$(4.2) \quad h_2 = a_1(\bar{\epsilon}_p)^{b_1} \exp(c_1\bar{\epsilon}_p).$$

- Shifted hyperbolic tangent

$$(4.3) \quad h_3 = a_1 [1 + \tanh(b_1 \bar{\epsilon}_p + c_1)].$$

The second material function g describing the growth of microvoids must be uniformly equal to 1 when initial void or voids are isolated in an unbounded matrix. It means that voids do not interact, no nucleation of new voids and no coalescence of voids in the growth process are considered. Those three phenomena are closely interrelated and can occur simultaneously. Unfortunately, the mechanical interpretation of the parameters is not so clear for that function.

We have tested two general functions g :

- exponential function

$$(4.4) \quad g_1(\bar{\epsilon}_p, a_2, b_2, c_2) = a_2 \exp [b_2 (\bar{\epsilon}_p)^{c_2}],$$

- square form of function g

$$(4.5) \quad g_2 = a_2 \sqrt{(\bar{\epsilon}_p)^2 + b_2 (\bar{\epsilon}_p) + c_2},$$

- hyperbolic function

$$(4.6) \quad g_3 = \frac{a_2}{b_2 - \bar{\epsilon}_p},$$

- constant function with constant equal to 1

$$(4.7) \quad g_4 \equiv 1,$$

- constant function with the identified constant

$$(4.8) \quad g_5 = a_2,$$

- linear function

$$(4.9) \quad g_6 = a_2 + b_2 * \bar{\epsilon}_p.$$

In the formulae introduced above $a_1, b_1, c_1, a_2, b_2, c_2$ are the unknown parameters.

We have tested all possible combinations of functions h and g . The meaning of particular cases is summarized in Table 1.

This means that for instance, Case A1 corresponds to the identification with the Gauss normal distribution function used as the nucleation material function h and exponential function used as the material growth function g .

Table 1. Summary of cases notation

	<i>g</i> -function					
	<i>g</i> ₁	<i>g</i> ₂	<i>g</i> ₃	<i>g</i> ₄	<i>g</i> ₅	<i>g</i> ₆
<i>h</i> ₁	A1	A2	A3	A4	A5	A6
<i>h</i> ₂	B1	B2	B3	B4	B5	B6
<i>h</i> ₃	C1	C2	C3	C4	C5	C6

5. BRIEF DESCRIPTION OF FISHER'S DATA USED FOR ESTIMATION

Our identification is based on the data prepared by FISHER [6]. In J.R.Fisher's experimental investigation, two carbon steels with 0.17 (type B) and 0.44 (type W) weight percent carbon, respectively, were used for the quantitative studies of microvoid nucleation and growth. The samples were subjected to the following sequence of heat treating operations. Rod sections of approximately 0.0826m in length were austenitized at 50°C above the A_3 temperature for 1.5 hours. The austenitized specimens were then rapidly quenched in ice water in order to obtain fine bainitic or martensitic structures. The quenched rods were then tempered at 700°C for a) 1 hour b) 24 hours and c) 120 hours, in order to obtain different particle size distributions in specimens of the same type. The heat-treated rods were machined into standard tensile specimens of 0.0254 m gage length and 0.0064 m diameter. All testing was done at room temperature. Metallographic observations were made on undeformed and deformed specimens using both the optical and electron microscopy. For each specimen, a series of transverse sections was prepared corresponding to successively smaller axial distances from the minimum cross-section. Each new section was obtained by grinding to the next premarked position and thus the previous sections were destroyed. Therefore, all data required from a given section had to be obtained before preparation of the succeeding one. Each section was carefully polished and etched after preliminary use of various grades of abrasive papers. The microstructural parameters were determined in both the deformed and undeformed specimens. For the deformed specimens the areal density of voids, η_A , and the volume fraction of voids, ξ , were obtained from transverse sections by standard metallographic techniques performed on scanning electron micrographs taken at a magnification of 2000 times. It is observed in Fisher's experiment that the voids tended to have elliptical cross-sections similar to those of the particles, as might be expected since the particles were nucleation sites for these voids. The total volume fraction of voids, ξ , and the nucleation part of volume fraction of voids, ξ^n , obtained by FISHER [6] are plotted as the function of equivalent plastic strain $\bar{\epsilon}_p$ in Fig. 1.

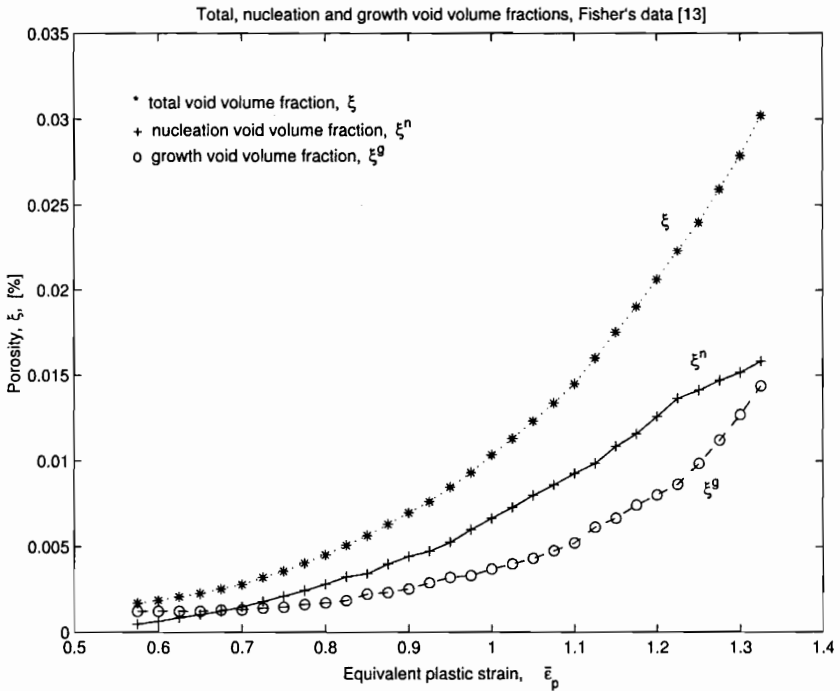


FIG. 1. Total void volume fraction, ξ (data from FISHER [6] for the B1-type steel) and the calculated void volume fraction due to nucleation, ξ^n , and due to growth, ξ^g , as a function of equivalent plastic strain, $\bar{\epsilon}_p$.

In Fisher's experimental work in the summary it was observed that:

- Voids are generally associated with particles of greater than average size. They are rarely formed at very small, isolated particles, even for the severe state of deformation which exists in the neck of a tensile specimen.
- Particles situated on ferrite grain boundaries are favored sites for the nucleation of voids.
- Voids often form by decohesion of the interfaces of particles which are closely spaced along the tensile axis.
- The maximum gradient in the void nucleation profile occurs at strains of $\bar{\epsilon}_p = 1.15$ and $\bar{\epsilon}_p = 0.80$ for B and W-type specimens, respectively.
- Voids elongate in the tensile direction but maintain elliptical cross-sections, indicating that plastic hole growth, and not the ferrite grain boundary separation, dictates the final void geometry.
- Non-equiaxial or irregularly shaped cementite particles are often subject to internal fracture. The resulting cracks tend to be oriented normally to the tensile direction and may sometimes be associated with boundaries between contiguous particles.

6. NUMERICAL METHODS

We have used the traditional least squares formulation of our identification problem. We minimize the mean squares error between the calculated and observed porosity values Eq. (2.2). Our earlier experience with the total porosity model [14] has presented the existence of many local minima in our problem. Therefore we have used for calculations our own implementation (standard ANSI C language) of the global minimization method of BOENDER, RINNOY KAN, TIMMER and STROUGIE in the form presented in TÖRN and ŽILINSKAS [21]. The details of the method are presented in [14]. In this paper we shall restrict it to the necessary minimum.

Locally we have used the BFGS quasi-Newton method with the numerical gradient estimation. The BFGS method is an unconstrained optimization method; however, in our implementation we have introduced box constraints on the parameters.

Our local minimizer makes use of a directional minimization method combining three different approaches – via the quadratic approximations along the search direction, cubic approximations and bisection. Paper [14] does not present its details. Therefore it is included here. Specific properties of the nonconvex unidirectional function has forced us to prepare a new switching condition between the three aforementioned approaches.

The third computational aspect is connected with the ordinary differential equation to be solved. It contains singularity in its right-hand side and it has led to difficulties with its numerical integration. The Runge-Kutta methods with automatic step-size selection has locked themselves in a kind of cycle. Therefore we have decided to choose the Rosenbrock method for stiff differential equations.

6.1. Global optimization method of Boender et al.

Global optimization method of BOENDER, RINNOY KAN, TIMMER and STROUGIE [2] was selected by us as the tool for solving our identification problem. To simplify the presentation let us assume that we consider the following optimization problem

$$(6.1) \quad \min_{\mathbf{x} \in V \subset R^n} f(\mathbf{x})$$

where: vector $\mathbf{x}^T = (a_1, b_1, c_1, a_2, b_2, c_2)$ (\mathbf{x}^T – denotes the transposition of the column vector \mathbf{x}), $n=6$ (sometimes 3 or 5), and V denotes the set of feasible values of parameters.

The global optimization method implemented by us belongs to the group of the so-called clustering methods and is a combination of sampling, clustering and local search.

Detailed structure of the algorithm:

- Step 0. Select N – number of sample points generated in one phase and γ – fraction of the sample points with the smallest function values. X^+ – the set of all local minima found so far; $X^{(1)}$ – the set of sample points leading to a minimum $x \in X^+$. Choose parameter $\epsilon_{Cl} > 0$ used in the clusterization.
- Step 1. Select N randomly generated points $\mathbf{x}^1, \mathbf{x}^2, \dots, \mathbf{x}^N \in V$. Let $f^i = f(\mathbf{x}^i)$ for $i = 1, \dots, N$.
- Step 2. Construct the transformed sample by taking the fraction γ lowest points of the current sample (their number is equal to N^+), performing one step of the steepest descent method and replacing those points by the resulting points. Drop the rest of the points.
- Step 3. Apply the clustering procedure to the transformed sample. The elements of X^+ (set of global points – local minima found up till now) are first chosen as seed points followed by the elements of $X^{(1)}$ (set of sample points leading to a minimum $x \in X^+$).
If all points $\mathbf{x}^1, \mathbf{x}^2, \dots, \mathbf{x}^{N^+}$ are classified then STOP, otherwise go to the next step.
- Step 4. For $i = 1, \dots, N^+$ do
if \mathbf{x}^i is classified neither to X^+ nor to $X^{(1)}$ then
a) apply the local search procedure starting from \mathbf{x}^i to obtain \mathbf{x}^{i+} ,
b) if $\mathbf{x}^{i+} \in X^+$ then add \mathbf{x}^i to $X^{(1)}$ (new seed point leading to an existing minimum),
c) if $\mathbf{x}^{i+} \notin X^+$ (\mathbf{x}^{i+} is a new local minimum) then add \mathbf{x}^{i+} to X^+ and \mathbf{x}^i to $X^{(1)}$.
- Step 5. Return to Step 1.

The described global optimization method characterizes convergence with probability one. It is typical for all methods involving stochasticity. Generally, involving stochastic elements, one sacrifices the possibility of an *absolute guarantee* of success. One can only get a result where the probability of sampling a point in the neighbourhood of the global optimum \mathbf{x}^* tends to 1 if the number of sample points in the global phase is increased. Under the notion “neighbourhood” we understand here the following set of points:

$$(6.2) \quad A^\epsilon(\mathbf{x}^*) = \{\mathbf{x} \in V; \|\mathbf{x} - \mathbf{x}^*\| \leq \epsilon\} \quad \text{for some } \epsilon > 0.$$

This result can be proved under mild assumptions on the minimized function and the sampling distribution. If the sampling distribution is uniform over V and function f is continuous, then the result is even stronger. Namely, the sample

point with the lowest function value tends to a point with minimal function value with probability 1.

Hence, the global phase could asymptotically guarantee the success. However, any method restricted only to sampling could be very time-consuming and would lack in efficiency. To increase the efficiency while maintaining the asymptotic guarantee of success is one of the challenges in the global optimization. In clustering methods one tries to increase efficiency by including the local search phase.

For clustering, a kind of a nearest neighbor method was used. The unclustered points are added to a cluster, initiated by a seed point either in X^+ or in $X^{(1)}$, if the distance to some point in the cluster is less than an a priori given distance ϵ_{C1} . Hence, accordingly, statements $\mathbf{x} \in X^+$ and $\mathbf{x} \in X^{(1)}$ should be understood in this way. As the result, we are storing local minimizers (X^+) and points leading to a minimizing point in $X^{(1)}$.

As the stopping criterion we require the fulfillment of one of the following conditions:

- all points from the transformed sample could be classified;
- either the number of local minima found or the number of points leading to a minimum is greater than their maximal permitted number;
- either the number of global minima found or the number of global seed points (i.e. sampling points leading towards a global minimum) is greater than the user-defined maximal value.

6.2. Local minimization method

As the local minimizer we have applied a specialized variant of the BFGS (Broyden, Fletcher, Goldfarb, Shanno) method for unconstrained optimization. It belongs to the class of the so-called quasi-Newton methods (see for instance FLETCHER [7], FINDEISEN *et al.* [5] or STACHURSKI and WIERZBICKI [20]).

The implemented algorithm is as follows:

Step 0. Specify bounds \mathbf{x}^L and \mathbf{x}^U on variables. Select a feasible starting point \mathbf{x}^0 satisfying the box constraints. Choose accuracy parameters $-\epsilon_{\text{BFGS}} > 0$, $\omega \in (0, 1)$. Calculate values of gradient \mathbf{p}^0 and function f^0 at the starting point \mathbf{x}^0 . Take $\mathbf{H}^0 = \mathbf{I}$ where \mathbf{I} is the identity matrix, $k := 0$.

Step 1. Calculate the current search direction according to the following formula:

$$\mathbf{d}^k = -\mathbf{H}^k \mathbf{p}^k.$$

Step 2. Find $\tau \leq 0$ such that the Armijo step-size rule is satisfied, i.e.

$$\frac{|(\nabla f(\mathbf{x}^k + \tau^k \mathbf{d}^k))^T \mathbf{d}^k|}{-(\nabla f(\mathbf{x}^k))^T \mathbf{d}^k} \leq \omega.$$

Step 3. Calculate the next point

$$\mathbf{x}^{k+1} = \mathbf{x}^k + \tau^k \mathbf{d}^k,$$

and the gradient \mathbf{p}^{k+1} at the new point.

Step 4. Check the stopping criterion (the Kuhn-Tucker conditions). If the stopping criteria are satisfied then STOP.

Step 5. Compute the gradient $\mathbf{r}^k = \mathbf{p}^{k+1} - \mathbf{p}^k$ and independent variables $\mathbf{s}^k = \mathbf{x}^{k+1} - \mathbf{x}^k$ differences. Update the approximation of the inverse Hessian using formula (6.4).

Step 6. Set $\mathbf{x}^{k+1} = \mathbf{x}^k$, $\mathbf{p}^{k+1} = \mathbf{p}^k$. Increase the iteration index k by one. Calculate $f(\mathbf{x}^k)$. Return to Step 1.

The original BFGS method starts from a given starting point \mathbf{x}^0 and realizes typical for the gradient unconstrained optimization steps of the form

$$(6.3) \quad \mathbf{x}^{k+1} = \mathbf{x}^k + \tau^k * \mathbf{d}^k,$$

where $\mathbf{d}^k = -\mathbf{H}^k \nabla f(\mathbf{x}^k)$ is the search direction and τ^k is the stepsize coefficient selected in the directional minimization function. It utilizes the gradient and independent variables differences to update the approximation \mathbf{H}^k of the inverse of the second-order derivative $(\nabla^2 f(\mathbf{x}^k))^{-1}$ of the minimized function according to the following formula:

$$(6.4) \quad \mathbf{H}^{k+1} = \mathbf{H}^k + \left(1 + \frac{(\mathbf{r}^k)^T \mathbf{H}^k \mathbf{r}^k}{(\mathbf{r}^k)^T \mathbf{s}^k} \right) \frac{\mathbf{s}^k (\mathbf{s}^k)^T}{(\mathbf{r}^k)^T \mathbf{s}^k} - \frac{\mathbf{s}^k (\mathbf{r}^k)^T \mathbf{H}^k + \mathbf{H}^k \mathbf{r}^k (\mathbf{s}^k)^T}{(\mathbf{r}^k)^T \mathbf{s}^k}$$

where $\mathbf{r}^k = \mathbf{p}^{k+1} - \mathbf{p}^k$, $\mathbf{s}^k = \mathbf{x}^{k+1} - \mathbf{x}^k$ and $\mathbf{p}^k = \nabla f(\mathbf{x}^k)$.

Iterations of the local minimizer are stopped when the norm of the gradient (derivative) of function f is smaller than a given accuracy $\epsilon_{\text{BFGS}} > 0$. In the directional minimization we have used successive quadratic approximations of function $\bar{f}(\tau) = f(\mathbf{x}^k + \tau * \mathbf{d}^k)$. Search along the direction is stopped when the so-called **Armijo step-size rule** is satisfied, i.e.

$$(6.5) \quad \frac{|d\bar{f}(\tau^k)|}{-d\bar{f}(0)} = \frac{|(\nabla f(\mathbf{x}^k + \tau^k \mathbf{d}^k))^T \mathbf{d}^k|}{-(\nabla f(\mathbf{x}^k))^T \mathbf{d}^k} \leq \omega, \quad \text{for some } \omega \in (0, 1).$$

Parameters ϵ_{BFGS} and ω are specified by the user.

We have modified this general scheme of the minimizer to take into account the box constraints on variables. This is in accordance with the modern optimization routines which are usually implemented so that they minimize a function subject to box constraints, i.e. solve the problem

$$(6.6) \quad \begin{array}{ll} \min_{\mathbf{x} \in R^n} & f(\mathbf{x}) \\ \text{s.t.} & \mathbf{x}_i^L \leq \mathbf{x}_i^U, \quad \text{for } i = 1, \dots, n. \end{array}$$

Our implementation is characterized by the following features:

- We maintain the inverse Hessian approximation in the whole space;
- Generate the descent direction in the whole space;
- Carry out the directional minimization in a specific way.

This differentiates substantially our approach from the typical active set method for problems with linear constraints.

It was also necessary to modify the stopping criterion. The Kuhn-Tucker necessary optimality conditions in the case of the box constraints take the form:

(i) The following inequalities should be satisfied on the boundaries

$$\begin{array}{ll} \text{if } x_i^{k+1} = x_i^L & \text{then } p_i^{k+1} \geq 0, \\ \text{if } x_i^{k+1} = x_i^U & \text{then } p_i^{k+1} \leq 0, \\ \text{for } & i = 1, \dots, n. \end{array}$$

(ii) The norm of the gradient in the subspace of variables that are not on their bounds in the new point \mathbf{x}^{k+1} should be equal to $\mathbf{0}$. Of course, in practice we verify whether it is sufficiently small.

6.3. Directional minimization

As we have seen in the previous subsection, it is necessary to minimize function f along the the search direction \mathbf{d}^k at each iteration, i.e. to solve the following problem:

$$(6.7) \quad \min_{\tau \geq 0} \bar{f}(\tau) = f(P(\mathbf{x}^k + \tau \mathbf{d}^k))$$

where P represents the projection operator on the set of feasible points defined by the box constraints.

Function \bar{f} is not necessarily convex. Typical gradient directional minimization algorithms make use either of the quadratic or the cubic approximations of function \bar{f} . They are usually based

- in the case of quadratic approximation – on function values at two points and gradient value at one of them

- in the case of cubic approximation – on function and gradient values in two points.

They are numerically correct if they are not too close to the linear approximation. If the second point τ is very close to the tangent line to the \bar{f} function graph at the first point τ_L , then the best quadratic or cubic approximation is the linear one. Furthermore, if \bar{f} is convex for $\tau \geq \tau_L$ close to τ_L then, in our opinion, quadratic approximation is the best one and in the opposite case – the cubic approximation. Therefore we have decided to verify the placement of τ and $\bar{f}(\tau)$ with respect to the above mentioned tangent line. We select quadratic approximation when point $\tau, \bar{f}(\tau)$ lies significantly above the tangent line, cubic approximation if it lies significantly below, and bisection if none of those two placements occurs.

Therefore, the choice depends on the mutual relation between the function value in the new trial point τ and value of the function linearization built in the left-hand bound of the search interval τ_L calculated at the same point ($\tau > \tau_L$)

- Cubic approximation if

$$(6.8) \quad \bar{f}(\tau_L) + (1 + \rho)\tau\bar{f}'(\tau_L) > \bar{f}(\tau).$$

- Bisection if

$$(6.9) \quad \bar{f}(\tau_L) + (1 + \rho)\tau\bar{f}'(\tau_L) \leq \bar{f}(\tau) \leq \bar{f}(\tau_L) + (1 - \rho)\tau\bar{f}'(\tau_L).$$

- Quadratic approximation if

$$(6.10) \quad \bar{f}(\tau) > \bar{f}(\tau_L) + (1 - \rho)\tau\bar{f}'(\tau_L).$$

The introduced selection criterion is very similar in its geometrical interpretation to the famous GOLDSTEIN conditions (cf. [5, 7, 8, 20]) used as the stopping criterion in many directional search algorithms. However, in the GOLDSTEIN tests the two linear cuts are above the tangent line and they serve a completely different purpose – to stop the directional minimization.

As the stopping criterion in our directional minimization routine we have used the so-called Armijo step-size rule. It has been formulated above (see formula 6.5). Therefore let us omit it here.

6.4. Integration of the ordinary differential equation

The considered model has the form of an ordinary differential equation. The right-hand side of Eq. (3.1) contains a singularity. Presence of the term $\frac{1}{1-\xi}$ causes the right-hand side to vary rapidly when ξ approaches 1. Generally, it has appeared that our equation is stiff and standard Runge-Kutta methods with

automatic selection of the step-size coefficients failed in our calculations. Obviously, we could apply a Runge-Kutta method with constant step-size, however we have decided to postpone that possibility due to the difficulties with the accuracy specification.

As a result, we have assumed that our equation is stiff and selected a Rosenbrock method for solving stiff sets of ordinary differential equations (see Numerical Recipes [17]).

7. NUMERICAL RESULTS

We did not know the precise range of material parameters. Therefore we have assumed at the beginning a broad range of feasible parameters, e.g.:

Case							
A1:	0.01	$\leq a_1 \leq$	0.05,	0.2	$\leq b_1 \leq$	0.6,	0.9 $\leq c_1 \leq$ 1.3
	1.0	$\leq a_2 \leq$	1.5,	0.01	$\leq b_2 \leq$	0.3,	0.01 $\leq c_2 \leq$ 0.2
B1:	0.0001	$\leq a_1 \leq$	0.1,	1.0	$\leq b_1 \leq$	1.5,	1.0 $\leq c_1 \leq$ 1.4
	0.01	$\leq a_2 \leq$	0.6,	0.1	$\leq b_2 \leq$	0.5,	0.8 $\leq c_2 \leq$ 1.0
C1:	0.001	$\leq a_1 \leq$	0.1,	2.5	$\leq b_1 \leq$	5.0,	-4.0 $\leq c_1 \leq$ 0.01
	1.0	$\leq a_2 \leq$	2.5,	3.0	$\leq b_2 \leq$	4.5	

At the next steps we have used small intervals containing the previously found optimal values of parameters as their new feasible ranges. The presented approach is a final result of our long experience with older variants of the program. We have encountered many computational difficulties during our experiments. Numerical difficulties encountered in the integration of the differential equation were the most serious problem in our calculations. Furthermore, at the beginning we did not know the range of the identified parameters. We know only some mechanical interpretation of the normal distribution h function. Such interpretation does not exist with respect to other forms of h function and all forms of the g function. In such situation it was also impossible to know in advance the range of the parameters. The bounds presented above we have obtained via a long process of computational attempts.

The results are collected in Tables 2 and 3 with all the tested cases A1–A6, B1–B6 and C1–C6. We have included for each case only the information on the three best minima found. Each line of Table 2 contains the following information about a minimum:

- the functional values,
- the corresponding values of parameters.

We are dealing with a statistical information and the problem of finding the best fitting model of the nucleation and voids growth phenomena. It is common

in estimation problems to add some statistical indicators pointing whether the model fits well the data from the statistical point of view.

Table 3 contains the corresponding, frequently used statistical information:

- Standard deviation s_e , where

$$(7.1) \quad s_e^2 = \frac{\left[\sum_{i=1}^M (Y_i - \tilde{Y}_i)^2 \right]}{M}$$

where: M is the number of observations,
 Y_i are the observed values of the output,
 \tilde{Y}_i are the calculated values of the output

$$(7.2) \quad \tilde{Y}_i = F(\bar{\epsilon}_{pi}, \mathbf{x}) \text{ for } i = 1, \dots, M.$$

- Weighted standard error s_{ew}

$$(7.3) \quad s_{ew} = \frac{s_e}{\bar{Y}},$$

where \bar{Y} is the mean value of the observed output

$$(7.4) \quad \bar{Y} = \frac{\left[\sum_{i=1}^M Y_i \right]}{M}.$$

- Correlation coefficient $r_{\mathbf{Y}\tilde{\mathbf{Y}}}$ between the observed and calculated output:

$$(7.5) \quad r_{\mathbf{Y}\tilde{\mathbf{Y}}} = \frac{\sum_{i=1}^M (Y_i - \bar{Y}) (\tilde{Y}_i - \bar{\tilde{Y}})}{\left[\sum_{i=1}^M (Y_i - \bar{Y})^2 \right]^{\frac{1}{2}} \left[\sum_{i=1}^M (\tilde{Y}_i - \bar{\tilde{Y}})^2 \right]^{\frac{1}{2}}},$$

where $\bar{\tilde{Y}}$ is the mean value of the calculated output

$$(7.6) \quad \bar{\tilde{Y}} = \frac{\left[\sum_{i=1}^M \tilde{Y}_i \right]}{M}.$$

Correlation close to 1 points that \mathbf{Y} and $\tilde{\mathbf{Y}}$ are well correlated.

- Values of the t -criterion, i.e.

$$(7.7) \quad t_s = \frac{\bar{z}}{S_z} \sqrt{M-1},$$

where

$$(7.8) \quad \bar{z} = \frac{\left[\sum_{i=1}^M z_i \right]}{M},$$

$$(7.9) \quad z_i = Y_i - \tilde{Y}_i,$$

and

$$(7.10) \quad S_z^2 = \frac{\left[\sum_{i=1}^M z_i^2 - \frac{(\sum_{i=1}^M z_i)^2}{M} \right]}{(M - 1)}.$$

This last value allows us to test the hypothesis that the expectation of the error $\mathbf{z} = \mathbf{Y} - \tilde{\mathbf{Y}}$ is equal to zero under the assumption that the error distribution is normal and σ^2 is unknown (see AFIFI and AZEN, [1]). In such a case t_s determined by formula (7.7) has the Student t-distribution with $M - 1$ degrees of freedom. Let $\theta = E(\mathbf{z})$ be the expectation of \mathbf{z} . We test the H_0 hypothesis that the expectation θ is equal to zero, i.e. $H_0 : \theta = 0$. As the alternative hypothesis $H_1 : \theta \neq 0$ is used. Then the P -value is

$$(7.11) \quad P = 2\text{Pr}(t(\nu) > |t_o|).$$

Hypothesis H_0 is rejected if $P < \kappa$, where κ denotes the level of significance. Instead of (7.8), one can check equivalently whether t_s belongs to the interval

$$(7.12) \quad (-t_{1-\kappa/2}(M - 1), t_{\kappa/2}(M - 1)),$$

where $t_{1-\kappa/2}(M - 1)$ denotes the critical value with the level of significance equal κ . For $M = 30$ and the level of significance $\kappa = 0.1$, the critical value is

$$(7.13) \quad t_{1-\kappa/2}(29) = 1.697.$$

We have depicted some of the results graphically in Figs. 2 and 3. Figure 2 presents the resulting dependence of the total porosity differences (observed minus the calculated values) with respect to the equivalent plastic strain $\bar{\epsilon}_p$ for all Cases A. Figures 3 (a - f) contain graphs of material functions h and g showing the dependence of their values with respect to the equivalent plastic strain $\bar{\epsilon}_p$.

Table 2. Identified parameters and fitting errors for the cases A1 - A6, B1 - B6, C1 - C6; h - nucleation functions with a_1, b_1 and c_1 ; g - growth functions with a_2, b_2 and c_2

Case	a_1	b_1	c_1	a_2	b_2	c_2	f
1	2.081212e-02	3.203613e-01	1.142677e+00	1.048110e+00	1.540339e-01	5.887020e-01	1.700284e-07
2	2.459752e-02	3.417624e-01	1.193470e+00	1.100321e+00	6.501482e-02	1.941033e-01	1.870735e-07
3	2.073352e-02	3.246460e-01	1.146024e+00	1.052570e+00	1.627909e-01	1.541159e-01	2.013667e-07
4	2.819688e-02	3.290185e-01	1.187475e+00	5.039920e-01	1.021578e+00	1.688143e+00	1.893821e-07
5	2.794326e-02	3.427333e-01	1.193001e+00	5.362410e-01	1.092745e+00	1.430616e+00	1.984865e-07
6	3.177080e-02	3.360531e-01	1.216207e+00	4.689406e-01	1.144043e+00	1.563800e+00	2.007179e-07
7	2.412438e-02	3.145564e-01	1.148306e+00	2.461575e+00	3.356563e+00		1.662608e-07
8	2.682749e-02	3.690178e-01	1.200510e+00	2.393928e+00	3.208201e+00		4.727793e-07
9	3.609856e-02	3.933141e-01	1.275095e+00	2.547901e+00	3.755815e+00		1.028279e-06
10	3.505692e-02	3.666815e-01	1.282348e+00				1.983268e-07
11	3.065935e-02	3.348365e-01	1.227703e+00				2.887013e-07
12	3.100329e-02	3.470957e-01	1.232653e+00				4.546674e-07
13	2.657334e-02	3.473849e-01	1.214838e+00	1.142003e+00			1.788396e-07
14	2.447573e-02	3.233043e-01	1.178914e+00	1.134999e+00			2.451784e-07
15	3.740360e-02	3.533577e-01	1.278640e+00	9.023870e-01			2.818601e-07
16	2.563980e-02	3.317624e-01	1.178424e+00	7.627987e-01	3.095568e-01		1.695705e-07
17	1.862920e-02	2.969529e-01	1.091176e+00	7.654488e-01	4.380955e-01		2.032952e-07
18	1.286682e-02	2.446338e-01	1.003067e+00	8.499793e-01	4.991069e-01		2.139974e-07
19	1.548730e-02	1.829196e+00	5.966584e-01	8.291838e-01	7.157868e-02	2.912159e-01	1.007905e-06
20	1.642854e-02	1.897919e+00	6.861903e-01	6.229555e-01	1.044736e-01	3.917156e-01	1.164333e-06
21	1.294056e-02	1.607321e+00	6.287958e-01	9.292985e-01	1.462683e-01	2.302958e-01	1.471906e-06
22	1.634198e-02	1.747208e+00	6.708150e-01	3.888362e-01	8.832497e-01	1.310916e+00	1.397040e-06
23	1.698248e-02	1.715469e+00	6.782495e-01	3.606531e-01	7.974402e-01	1.143107e+00	2.038704e-06
24	1.431830e-02	1.570579e+00	7.059013e-01	4.823660e-01	7.234962e-01	1.288154e+00	2.177861e-06
25	1.584352e-02	1.903237e+00	8.008182e-01	2.024103e+00	4.653833e+00		9.331585e-07
26	1.381212e-02	1.690606e+00	8.282727e-01	2.167394e+00	4.049697e+00		1.225122e-06
27	1.425329e-02	1.933893e+00	8.256529e-01	2.266634e+00	4.265744e+00		2.052942e-06

Table 3. Statistical results for the cases A1 - A6, B1 - B6, C1 - C6 se - standard deviation, sew - weighted standard error, $r_{Y\hat{Y}}$ - correlation coefficient, t_s - t -criterion

Case	se	sew	$r_{Y\hat{Y}}$	t -criterion
1	5.667615e-09	6.572061e-03	9.999637e-01	-8.864216e-01
2	6.235784e-09	6.884115e-03	9.999638e-01	-2.027278e+00
3	6.712223e-09	7.138756e-03	9.999649e-01	-2.404000e+00
4	6.312736e-09	6.935533e-03	9.999592e-01	-8.943711e-01
5	6.616216e-09	7.087291e-03	9.999649e-01	-2.456950e+00
6	6.690596e-09	7.147402e-03	9.999548e-01	-9.753891e-02
7	5.542027e-09	6.502675e-03	9.999630e-01	-4.06436e-01
8	1.575931e-08	1.092479e-02	9.999182e-01	-2.205599e+00
9	3.427596e-08	1.597171e-02	9.999392e-01	-7.171233e+00
10	6.610892e-09	7.091231e-03	9.999589e-01	-1.579673e+00
11	9.623375e-09	8.571815e-03	9.999349e-01	-9.091713e-02
12	1.515558e-08	1.071005e-02	9.999251e-01	-2.465213e+00
13	5.961321e-09	6.740050e-03	9.999619e-01	-8.817724e-01
14	8.172614e-09	7.880864e-03	9.999507e-01	-1.757652e+00
15	9.395336e-09	8.464723e-03	9.999369e-01	-4.571680e-01
16	5.652350e-09	6.564784e-03	9.999631e-01	-6.871396e-01
17	6.776505e-09	7.175781e-03	9.999612e-01	-2.008447e+00
18	7.133247e-09	7.384449e-03	9.999521e-01	3.333976e-01
19	3.359683e-08	1.595189e-02	9.998283e-01	-1.429916e+00
20	3.881109e-08	1.699830e-02	9.998880e-01	-5.938166e+00
21	4.906353e-08	1.923160e-02	9.997048e-01	-1.904976e+00
22	4.635799e-08	1.860863e-02	9.998255e-01	-3.901448e+00
23	6.795680e-08	2.240796e-02	9.998653e-01	-5.696154e+00
24	7.259538e-08	2.318532e-02	9.997187e-01	-4.672584e+00
25	3.110528e-08	1.532762e-02	9.998493e-01	-2.055174e+00
26	4.083740e-08	1.757314e-02	9.997854e-01	-1.552465e+00
27	6.843140e-08	2.293090e-02	9.995485e-01	7.093460e-01

Table 3. [cont.]

28		4.535961e-08	1.840385e-02	9.998250e-01	-4.070490e+00
29	B4	4.809546e-08	1.893327e-02	9.998404e-01	-4.416692e+00
30		5.373734e-08	1.998720e-02	9.998534e-01	-4.784334e+00
31		3.876339e-08	1.707357e-02	9.998541e-01	-2.677776e+00
32	B5	4.549464e-08	1.852984e-02	9.998501e-01	-1.787203e+00
33		6.923523e-08	2.261579e-02	9.998598e-01	-5.646950e+00
34		5.117596e-08	1.951984e-02	9.998754e-01	-4.506494e+00
35	B6	5.295923e-08	1.991955e-02	9.997619e-01	-2.889709e+00
36		6.513467e-08	2.216006e-02	9.995955e-01	-1.609527e+00
37		7.669524e-09	7.641082e-03	9.999525e-01	-1.145540e+00
38	C1	8.817585e-09	8.173929e-03	9.999543e-01	-2.918241e+00
39		9.702364e-09	8.609684e-03	9.999510e-01	1.068294e-01
40		6.291975e-09	6.924098e-03	9.999600e-01	-8.982919e-01
41	C2	6.902130e-09	7.247827e-03	9.999590e-01	-1.310099e+00
42		7.372120e-09	7.483696e-03	9.999561e-01	-2.006045e+00
43		7.358126e-09	7.489766e-03	9.999517e-01	-6.364182e-01
44	C3	8.552350e-09	8.079605e-03	9.999423e-01	-1.895524e-01
45		1.181703e-08	9.511706e-03	9.999218e-01	6.872025e-01
46		6.581110e-09	7.078005e-03	9.999598e-01	-1.259035e+00
47	C4	7.019856e-09	7.305773e-03	9.999585e-01	-1.699784e+00
48		7.078294e-09	7.333948e-03	9.999618e-01	-1.944524e+00
49		6.377318e-09	6.975820e-03	9.999572e-01	-3.445298e-01
50	C5	6.585065e-09	7.087626e-03	9.999560e-01	-4.351406e-01
51		6.751998e-09	7.173355e-03	9.999565e-01	-8.019927e-01
52		6.592200e-09	7.091104e-03	9.999561e-01	-4.733982e-01
53	C6	6.615379e-09	7.105462e-03	9.999555e-01	-2.713799e-01
54		6.699170e-09	7.149989e-03	9.999549e-01	-3.041052e-01

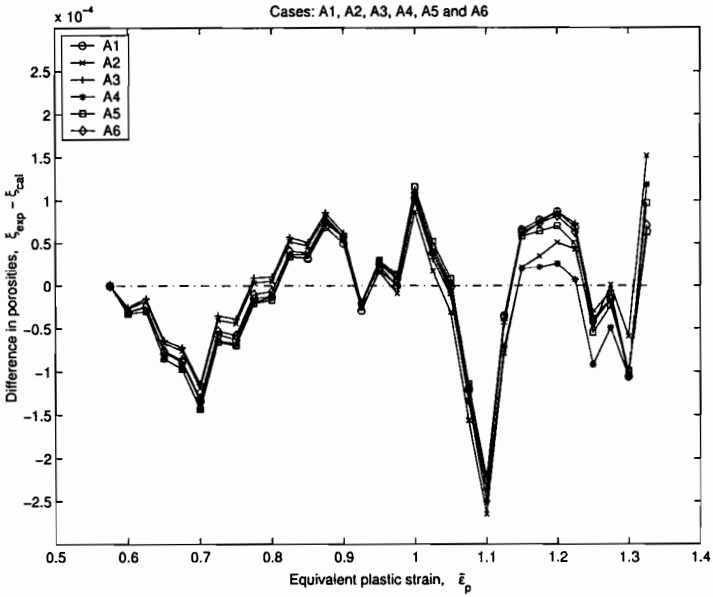


FIG. 2. Differences between the experimental and calculated total porosity versus equivalent plastic strain $\bar{\epsilon}_p$.

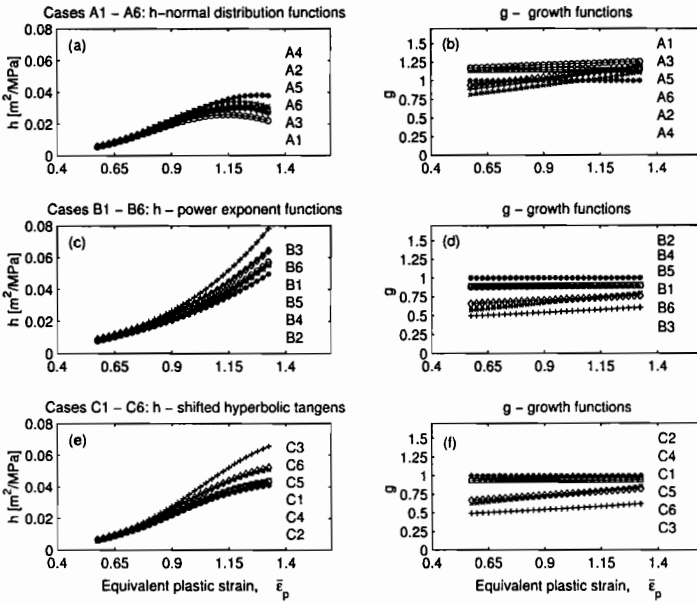


FIG. 3. Graphs of the material functions values with respect to the equivalent plastic strain $\bar{\epsilon}_p$.

8. CONCLUSIONS AND COROLLARIES

Our computational experiment has proved the existence of many local minima in our nonlinear regression problem. Many of them are acceptable with respect to the mean squares error taken by us as the fitting measure of the model. The best fitting error is of the order of 10^{-7} (see Table 2). Fitting error of order 10^{-7} we have observed in all cases assuming h equal to the Gauss distribution function (Cases A1–A6). The best results were observed in Cases A3, B3 and C3 (in all of them g was the hyperbolic function) – all best fitting errors were of order 10^{-7} . This leads to the corollary that hyperbola is the best choice for the growth function g . Among them the nucleation function h in the form of the Gauss distribution function seems to be the best selection.

We have found several other local minima of the least squares function which are slightly worse with respect to the fitting error. This fitting error is also relatively good (from 10^{-6} to 10^{-5}) and the parameters are reasonable from the mechanical point of view. Table 2 contains three of them for each particular case.

Cases A1, A2, A3, B1, B2, B3, C1, C2 and C3 suggest (see Fig. 3) that it would be good to try to identify the model using constant function g (see Tables 2 and 3). In many cases function g was very flat. We have tried two variants. First constant $g \equiv 1$ with an *a priori* specified value of the constant. Value 1 has been suggested by many authors. Computational results indicate that material function $g \equiv 1$ is also a relatively good choice – the fitting error is only slightly worse (best error order is 10^{-7} in Case A4 and 10^{-6} in Cases B4 and C4). In the second variant we have decided to identify that constant, i.e. we have used $g_5 = a_2$. The identification has led to slightly unexpected by us result – constant value approximately equal to 0.84 smaller than 1. It is observed for all forms of the h functions. Of course, we should remember that it concerns only spheroidal mild steel used in Fisher's experiment. Unfortunately, we were not able to find similar data for other types of material. As the next step we plan to investigate another model – separating the nucleation and growth phenomena. However, they will also concern spheroidal steel materials.

We have investigated also the linear form of the growth function g . The trial has been successful. Fitting error in Case A6 was very similar to Case A1. In other cases the fitting error was only slightly worse. What is interesting, the mean value of that linear growth material function g is almost equal to the estimated constant value (see Cases A6 and A5, B6 and B5, C6 and C5).

Our identification results suggest also a kind of nonuniqueness in the parameter determination problem in its current setting. An open question is which one of the minima found should be accepted. At the present stage of research, only mechanical interpretations and conditions may suggest the best choice.

Another open question is the use of other measures of deviations of the calculated output from the measured one.

One should remember that in our considerations we have accepted some assumptions:

- The matrix material is plastically incompressible, $\dot{\rho}_m = 0$ and the elastic part of a strain rate tensor is neglected, $D_{ij} = D_{ij}^p$.
- The shape of the material function h is in agreement with the material function proposed by CHU and NEEDLEMAN [4]. However, the growth material function g , as in PERZYNA and NOWAK [16], can be not constant and has the form of an exponential function.

ACKNOWLEDGEMENTS

The work of Z.N. has been prepared in part within the framework of the research project KBN 7T08B02416.

REFERENCES

1. A. A. AFIFI, S. P. AZEN, *Statistical analysis. A computer oriented approach*, Academic Press, New York 1979.
2. C. G. BOENDER, A. H. G. RINNOOY KAN, L. STROUGIE, G. T. TIMMER, *A Stochastic method for global optimization*, *Mathematical Programming*, **22**, 125-140, 1982.
3. P. W. BRIDGMAN, *Studies in large plastic flow and fracture*, McGraw-Hill, 1952.
4. C. C. CHU, A. NEEDLEMAN, *Void nucleation effects in biaxially stretched sheets*, *Trans. ASME, J. Engng. Materials and Technology*, **102**, 249-256, July 1980.
5. W. FINDEISEN, J. SZYMANOWSKI, A. WIERZBICKI, *Theory and computational methods of optimization* [in Polish], PWN, Warszawa 1977.
6. J. R. FISHER, *Void nucleation in spheroidized steels during tensile deformation*, Ph.D. Thesis, Brown University, June 1980.
7. R. FLETCHER, *Practical methods of optimization, second edition*, John Wiley & Sons, Chichester 1987.
8. A. A. GOLDSTEIN, *On steepest descent*, *SIAM J. Control*, **3**, 147-151, 1965.
9. A. L. GURSON, *Continuum theory of ductile rupture by void nucleation and growth. Part 1. Yield criteria and flow rules for porous ductile media*, *J. Engng. Materials and Technology, Trans. of the ASME*, **99**, 2-15, 1977.
10. R. HILL, *Mathematical plasticity*, Oxford Press, 1950.
11. K. LEVENBERG, *A Method for the solution of certain nonlinear problems in least squares*, *Quart. Appl. Math.*, **2**, 164-168, 1944.
12. D. W. MARQUARDT, *An algorithm for least squares estimation of nonlinear parameters*, *SIAM Journal on Applied Mathematics*, **11**, 431-441, 1963.

13. A. NEEDLEMAN, J. R. RICE, *Limits to ductility set by plastic flow localization*, D.P. KOISTINEN, N. M. WANG, [Eds.], *Mechanics of Sheet Metal Forming*, 237-267, Plenum, New York 1978.
14. Z. NOWAK, A. STACHURSKI, *Global optimization in material functions identification for voided media plastic flow*, submitted for publication in *CAMES*, 2002.
15. P. PERZYNA, *Internal state variable description of dynamic fracture of ductile solids*, *Int. J. Solids Structure*, **22**, 797-818, 1986.
16. P. PERZYNA, Z. NOWAK, *Evolution equation for the void fraction parameter in necking region*, *Arch. Mech.*, **39**, No. 1-2, 73-84, 1987.
17. W. H. PRESS, S. A. TEUKOLSKY, W. T. VETTERLING, B. P. FLANNERY, *Numerical recipes in C: The art of scientific computing*, Cambridge University Press, Cambridge 1993.
18. J. W. RUDNICKI, J. R. RICE, *Conditions for the localization of deformation in pressure-sensitive dilatant materials*, *Journal Mech. Phys. Solids*, **23**, 371-394, 1975.
19. M. SAJE, J. PAN, A. NEEDLEMAN, *Void nucleation effects on shear localization in porous plastic solids*, *Int. J. Fracture*, **19**, 163, 1982.
20. A. STACHURSKI, A. P. WIERZBICKI, *Introduction to optimization* [in Polish], Publishing House of the Warsaw University of Technology, Warsaw 1999.
21. A. TÖRN, A. ŽILINSKAS, *Global optimization*, Springer Verlag, Berlin, Heidelberg 1989.

Received December 29, 2000.
